AIAA JOURNAL
Vol. 44, No. 2, February 2006

Quasi-One-Dimensional Model for Realistic Three-Dimensional Synthetic Jet Actuators

N. K. Yamaleev*
North Carolina A&T State University, Greensboro, North Carolina 27411
and
M. H. Carpenter†
NASA Langley Research Center, Hampton, Virginia 23681

A systematic methodology for approximating realistic three-dimensional synthetic jet actuators by using a reduced-order model based on the time-dependent compressible quasi-one-dimensional Euler equations is presented. The following major questions are addressed: 1) which three-dimensional actuator geometries are amenable to the quasi-one-dimensional approximation; 2) which three-dimensional actuator parameters should be retained in the quasi-one-dimensional model; 3) which actuator flow regions are essentially multidimensional and are not candidates for reduced-order modeling; and 4) which geometrical features practically do not contribute to the fidelity of the actuator solution. Constraints that should be imposed on the actuator geometry and the flow parameters are discussed. The accuracy of the quasi-one-dimensional model is validated by comparing the numerical results with experimental data and full time-dependent Navier–Stokes simulation of the same realistic actuator.

I. Introduction

AMONG various flow control methods, periodic excitation of a basic flow via synthetic jet actuation is the most promising technique that demonstrates the great potential for active flow control.[1–3] Synthetic jet actuation can provide flexibility in design and stability to moderate perturbations in the exterior flowfield, as well as adaptability to a larger operating envelope. Numerical solution of this very important class of problems is extremely computationally expensive. The computational cost of a typical discretization of the time-dependent three-dimensional full Navier–Stokes model is generally too large for design and optimization studies. Hence, reduction in the complexity of the full model described by the Navier–Stokes equations is necessary.

Several approaches for simulation of synthetic jet actuators are available in the literature. All of the methods can be divided into two classes: 1) simplified transpiration boundary conditions and lumped element models[4,5] that do not simulate the flow inside the actuator cavity, and 2) full numerical simulation of both the exterior and cavity flows.[6–8] Although the methods just mentioned have been successfully used for modeling synthetic jet flows, there are several problems that make them practically inapplicable to optimization of the actuator performance. One of the main drawbacks of the simplified boundary conditions is that they do not satisfy the conservation laws. Another disadvantage of the zero-order models is their inability to account for the geometry and size of the actuator, viscous effects associated with the flow through the orifice, and changes in the pressure field caused by the interaction of the external boundary layer and the actuator. The major drawbacks of the lumped element models are caused by the use of the incompressible unsteady pipe flow theory to describe the flow inside the actuator neck and the assumption that the flow near the orifice exit is fully developed. As a result, these models neglect compressibility effects associated with large-amplitude pressure oscillations in the orifice and overpredict viscous losses in the neck region. The main problem associated with the second class of methods is huge computational cost. On one hand, the numerical calculation of the cavity flow requires at least the same number of grid points needed to solve the exterior flowfield. On the other hand, the Mach number in the problem varies from $\mathcal{O}(10^{-3})$ (near the diaphragm) to $\mathcal{O}(1)$ (in the exterior flow). The variation of the flow parameters from fully incompressible to fully compressible regimes and the presence of the moving boundary considerably increase the algorithm complexity. As a result, the full numerical simulation methods are extremely expensive in terms of computational time and therefore practically inapplicable in optimization studies.

The main objective of this paper is to further develop the systematic methodology for approximating realistic three-dimensional synthetic jet actuators by using the quasi-one-dimensional reduced-order model that was originally proposed in Ref. 9. As has been shown in Ref. 9, the new quasi-one-dimensional model is more than 1.5 times faster than the full two-dimensional numerical simulation method, while providing near full fidelity in the exterior flowfield. These results have been obtained under the assumption that the quasi-one-dimensional actuator geometry exactly coincides with that of the realistic actuator. The analysis and numerical results presented here demonstrate that this geometrical constraint can be removed if the actuator size is much smaller than the wavelength of diaphragm vibrations, which is true for a very broad class of realistic actuators. Another very important question discussed in the present paper is what parameters and geometrical features of a realistic actuator make the major contribution to the fidelity of the actuator solution and should therefore be retained in the quasi-one-dimensional model.

II. Solution Methodology

The solution methodology used for this work is described in detail elsewhere.[9] Only the general aspects of the approach will be replicated herein. The time-dependent compressible two-dimensional Navier–Stokes equations are used to describe the unsteady airflow generated by a synthetic jet actuator. In the present analysis, the following two problems are solved: a synthetic jet actuator pulsing into quiescent air and interaction of the same actuator with a crossflow. In both test cases, the Reynolds number based on the actuator orifice size and the peak velocity at the jet exit is of the order of 2.8×10^3. Therefore, the flow in the entire domain is assumed to be laminar, and no turbulence model is used in these simulations. The governing equations in curvilinear coordinates are written in conservation law

Received 8 November 2004; revision received 20 June 2005; accepted for publication 21 June 2005.

*Associate Professor, Department of Mathematics; nkyamale@ncat.edu. Member AIAA.
†Senior Research Scientist, Mail Stop 128, Computational Aeroscience Branch.

form. All of the length scales and dependent variables have been nondimensionalized by the orifice width d and the corresponding reference values, respectively, except for pressure which has been normalized by $\rho_\infty u_\infty^2$. In the case of the quiescent flow, ρ_∞ is the density of the ambient fluid and u_∞ is the reference velocity, which has been chosen to be one-tenth of the speed of sound. For the cross-flow problem, ρ_∞ and u_∞ are the freestream density and velocity, respectively. The viscosity coefficient is assumed to be constant, and the equation of state for a perfect gas is used to relate pressure to the conservation variables. Details of the implementation of the boundary conditions are discussed in Sec. V.

The actuator geometry is represented as the summation of multiple subdomains, each having a high degree of smoothness. Within each subdomain, a computational grid is generated having sufficient smoothness to provide the metric coefficients with three significant digits of accuracy. The connectivity at the subdomain interfaces is C_0 smooth; thus, mesh lines connect at interfaces but need not have smooth derivatives. A fourth-order upwind-biased linear finite difference scheme based on the local Lax–Friedrichs flux splitting is used to discretize both the two-dimensional Navier–Stokes equations and the quasi-one-dimensional Euler equations. For sufficient grid smoothness within each two-dimensional subdomain, design order accuracy is achieved. The interfaces are connected using the penalty approach described in detail in Refs. 10–12. The interface penalty treatment is conservative and maintains the underlying accuracy of the interior scheme. The penalty procedure requires colocated solution variables on both sides of the interface. In other words, the solution is discontinuous along the interfaces, but the jump in the solution values is of the order of the truncation error of the numerical scheme used. The L_2 norm of the difference between these two solution values at each interface is used as a measure of spatial grid resolution. For all of the simulations presented, the interface error is less than 0.5%.

The semidiscrete equations are explicitly integrated in time with a low-storage fourth-order Runge–Kutta scheme.[13] The simulations are all run at the maximum stable time step. The temporal scheme has an error estimator that monitors the temporal error per time step. The temporal error varies over the period in the range 10^{-10}–10^{-7}, based on the L_∞ norm of the density variable. Other solution variables have similar error norms. Each cycle requires about 10^5 time steps to complete.

III. Quasi-One-Dimensional Model

A key idea of the reduced-order model is to simulate the flow inside the actuator cavity by using the time-dependent compressible quasi-one-dimensional Euler equations. The quasi-one-dimensional Euler equations in the time-dependent coordinate frame (τ, ζ) can be written in conservation law form as follows:

$$\frac{\partial \bar{\boldsymbol{U}}}{\partial \tau} + \frac{\partial \bar{\boldsymbol{E}}}{\partial \zeta} + \bar{\boldsymbol{H}} = 0$$

$$\bar{\boldsymbol{U}} = \frac{A}{J}\begin{bmatrix} \rho \\ \rho v \\ \rho e \end{bmatrix}, \qquad \bar{\boldsymbol{E}} = \frac{A}{J}\begin{bmatrix} \zeta_t \rho + \zeta_y \rho v \\ \zeta_t \rho v + \zeta_y (\rho v^2 + p) \\ \zeta_t \rho e + \zeta_y v(\rho e + p) \end{bmatrix}$$

$$\boldsymbol{H} = -\frac{1}{J}\begin{bmatrix} 0 \\ p\dfrac{\partial A}{\partial y} \\ 0 \end{bmatrix}$$

$$y(\zeta, \tau) = (1-\zeta)\{L + a[1 - \cos(\omega\tau)]\}, \qquad J = \frac{1}{y_\zeta} \tag{1}$$

where A is the cross-sectional area of the quasi-one-dimensional actuator, which is assumed to be independent on time, a and ω are the diaphragm amplitude and frequency, respectively, and $L + a$ is a mean depth of the quasi-one-dimensional actuator. Note that the ζ coordinate depends on time, and, therefore, a moving mesh technique is applied to solve the quasi-one-dimensional Euler equations. Diaphragm oscillations are forced by varying the position of the diaphragm $y(0, \tau)$, where the impermeable wall boundary condition is imposed. The diaphragm velocity is calculated by differentiating y with respect to time to give $v(0, \tau) = a\omega \sin(\omega\tau)$.

A region near the jet exit requires special consideration. The full numerical simulation of the actuator orifice region is crucial for accurate prediction of the interaction between the synthetic jet and the exterior flow. This region is characterized by strong flow separation that cannot be described by the quasi-one-dimensional Euler equations.[9] Therefore, the small region near the actuator orifice is modeled by solving the two-dimensional compressible unsteady Navier–Stokes equations, whereas the flow inside the actuator cavity is described by the quasi-one-dimensional Euler equations (1). This approach allows us to accurately predict the interaction of the synthetic jet with the external flow and to resolve vortices generated in the vicinity of the actuator orifice, while reducing the computational cost.

The low-dimensional actuator model possesses several advantages that make this approach very attractive. First, the quasi-one-dimensional model is fully conservative and provides conservation of mass, momentum, and energy. Furthermore, the reduced-order model is computationally much more efficient as compared with the two- or three-dimensional Navier–Stokes simulation of the cavity flow. These properties of the reduced-order model and its ability to account for the compressibility effects inherent in actuator devices can be efficiently used for quantitative prediction of the synthetic jet flows. However, the question that has not been addressed yet is which parameters of a realistic actuator make the major contribution to the fidelity of the actuator solution and should be retained in the quasi-one-dimensional model. This question is discussed in the next section.

IV. Approximation of Three-Dimensional Actuators by Using the Quasi-One-Dimensional Model

In our previous study,[9] we showed that the quasi-one-dimensional model provides near full fidelity (2–3% error) in the exterior flowfield if the following constraints are met: 1) the quasi-one-dimensional actuator geometry exactly coincides with the real actuator geometry; 2) $Re_d \geq 500$, where Re_d is the Reynolds number based on the freestream flow parameters and the actuator orifice size d; and 3) the interface between the quasi-one-dimensional Euler equations and two-dimensional Navier–Stokes equations should be located at least $2d$ away from the orifice exit. For realistic actuators, Re_d is of the order of $\mathcal{O}(10^3)$, and the quasi-one-/two-dimensional interface is a user-defined parameter. Therefore, the second and third constraints can readily be satisfied for a broad class of synthetic jet actuators. However, the first constraint imposes a severe restriction on the actuator geometry, which abandons the applicability of the quasi-one-dimensional model to the simulation of realistic three-dimensional actuators. In connection with this, we will discuss three considerations indicating that the quasi-one-dimensional model can quantitatively predict the realistic three-dimensional actuator dynamics.

The first observation is that the size of a realistic actuator is much less than the wavelength of diaphragm vibration. Actually, the actuator size is determined by the size of a wing, blade, or other control surfaces where the actuator is embedded. The actuator characteristic size can be evaluated as follows: $L_a = V_a/S_a$, where V_a and S_a are the actuator volume and internal surface area, respectively. The characteristic length of the actuator considered in the present study is $\mathcal{O}(10^{-2})$ m, whereas the wavelength of diaphragm oscillations is

$$\lambda = \omega/c_\infty$$

where ω is the diaphragm frequency and c_∞ is the speed of sound. For centimeter-size actuators considered in this work, the diaphragm frequency is of the order of 1 kHz. Dividing L_a by λ yields

$$\frac{L_a}{\lambda} = \frac{V_a \omega}{S_a c_\infty} \approx \frac{10^{-2} \times 10^3}{3 \times 10^2} \approx 3 \times 10^{-2} \ll 1$$

As follows from the preceding estimate, the actuator characteristic size is much less than the diaphragm wavelength. All changes in

the pressure and velocity fields inside the actuator cavity occur on the scale of the wavelength of diaphragm vibration and, therefore, are by a factor L_a/λ less than the pressure and velocity themselves. Another conclusion that can be drawn from this consideration is that the cavity shape does not significantly effect the actuator performance if $L_a \ll \lambda$. However, the jet momentum strongly depends on the actuator volume and neck length. This property is discussed at the end of this section.

Another very important question that needs to be addressed is whether or not vortices ingested inside the actuator cavity have a strong effect on the actuator characteristics. One can speculate that because the exterior flow is essentially turbulent vortices generated in the turbulent boundary layer can be ingested into the actuator cavity, which makes the cavity flowfield substantially multidimensional. Assuming that an ingested vortex does not completely dissipate while going through the actuator neck, let us estimate the total vortex energy and compare it with the total energy of gas inside the actuator cavity. Because the maximum vortex diameter is bounded by the orifice size, the vortex energy can be estimated as follows:

$$E_{\text{vortex}} = \int_{V_{\text{vortex}}} \rho e \, \mathrm{d}V \approx \frac{\pi d^2}{4} L P_\infty \left[\frac{1}{\gamma - 1} + \frac{\gamma}{2} \left(\frac{M_o d}{D} \right)^2 \right] \quad (2)$$

where L is the slot length, M_o is the peak Mach number at the orifice exit, D is the diaphragm diameter, and V_{vortex} is the vortex volume. Equation (2) has been obtained under the following assumptions: the flow is two-dimensional and incompressible, and the amplitude of pressure oscillations is much less than P_∞, which is a direct consequence of the fact that the synthetic jet peak Mach number is $\mathcal{O}(10^{-1})$. The total energy of gas inside the cavity is

$$E_{\text{cavity}} = \int_{V_{\text{cavity}}} \rho e \, \mathrm{d}V \approx L_a^2 L P_\infty \left[\frac{1}{\gamma - 1} + \frac{\gamma}{2} \left(\frac{\omega a}{c_\infty^2} \right)^2 \right] \quad (3)$$

where L_a is the actuator characteristic size, L is a slot length, V_{cavity} is the cavity volume, and a is a diaphragm amplitude. Accounting for the fact that the kinetic energy in Eqs. (2) and (3) is much less than the corresponding internal energy term, one can write

$$E_{\text{vortex}}/E_{\text{cavity}} \approx d^2 \big/ L_a^2 \approx (10^{-3}/10^{-2})^2 = 10^{-2} \ll 1 \quad (4)$$

Note that in the three-dimensional case, because of the vortex breakdown, the ratio $E_{\text{vortex}}/E_{\text{cavity}}$ is of the order of $\mathcal{O}(d^3/L_a^3)$, which is more than an order of magnitude smaller than the estimate (4). Equation (4) shows that even if the vortex is ingested inside the cavity, its energy is much smaller than the total energy of the system and can therefore be neglected. Assuming that the problem under consideration is well-posed, one can conclude that the negligibly small perturbations in the energy of the system, caused by the vortex ingestion, result in negligibly small perturbations in the actuator solution.

The third very important consideration is independence of the actuator acoustic resonance frequency on the cavity shape. First of all, because of design constraints the diaphragm deflection is much less than the actuator characteristic size. As a result, the volume variation as a result of diaphragm oscillations is negligibly small as compared with the cavity volume. Therefore, the Helmholtz resonance theory can be applied to estimate the actuator resonance frequency, which is given by the following formula:

$$\omega \sim c_\infty \sqrt{S_o/Vl'} \quad (5)$$

where V is the actuator volume, l' is the characteristic neck length, S_o is the orifice cross-sectional area, and c_∞ is the speed of sound. From Eq. (5) it follows that the acoustic resonance frequency does not depend on the actuator shape, but does depend on the actuator volume V, neck length l', and orifice size d. Equation (5) indicates that to quantitatively predict the resonance characteristics of a three-dimensional actuator the following parameters of the realistic actuator, such as V, l', and d, should be retained in the quasi-one-dimensional model.

Summarizing what has just been said, we can conclude that to accurately approximate realistic three-dimensional actuators by using the quasi-one-dimensional model, the following constraints should be imposed:

1) The actuator size should be much smaller than the wavelength of diaphragm oscillation.

2) The cavity volume, neck length, slot size, diaphragm area, frequency, and amplitude of the quasi-one-dimensional model should be equal to those of the realistic three-dimensional actuator.

3) The Reynolds number based on the slot size should not be less than 500, and the quasi-one-/two-dimensional interface should be located more than $2d$ away from the orifice exit.

V. Implementation and Numerical Results

The following two problems are considered in this study: 1) a synthetic jet actuator pulsing into an initially quiescent flow and 2) interaction of the same actuator with a crossflow. The objective of the first problem is to compare our numerical results with the experimental data.[4] The main objective of the second problem is to quantify the magnitude of error committed by the reduced-order model, which is evaluated by comparing the numerical solutions obtained with the quasi-one-dimensional model and the full two-dimensional Navier–Stokes simulation of the same actuator.

A. Synthetic Jet in Quiescent Flow

In the experiment performed at NASA Langley Research Center (LaRC),[14] a synthetic jet in quiescent air is generated by a cavity-pumping actuator. The synthetic jet actuator consists of a slot 1.27 mm wide and 35.56 mm long and a narrow cavity. The slot is in the center of the bottom of an enclosed $609.6 \times 609.6 \times 609.6$ mm box and is parallel with the sides of the outer walls. The flow through the slot alternates between outflow and inflow, which is driven by a single piezoelectric diaphragm, 50.8 mm in diameter, mounted on the side of the cavity. The diaphragm is driven at 444.7 Hz, which is selected to operate away from the cavity resonance frequency of 500 Hz. In this experiment, three different techniques, hot-wire anemometry (HW), laser Doppler velocimetry (LDV), and particle image velocimetry (PIV), were used to measure the velocity field. Note that two sets of experimental data have been taken for this test case. The first set of data was used for the NASA LaRC workshop on "CFD Validation of Synthetic Jets and Turbulent Separation Control," and the other one was performed later at the conditions that slightly differ from those already mentioned. Although the later results show a better consistency between the HW, LDV, and PIV techniques, only the original workshop data are used in the present paper.

The exterior box and the neck portion of the actuator geometry used in the numerical simulation are obtained as a two-dimensional projection of the three-dimensional experimental setup. These regions are simulated by solving the two-dimensional time-dependent compressible Navier–Stokes equations. The actuator cavity is approximated with a quasi-one-dimensional nozzle geometry, so that the volume and diaphragm area of the quasi-one-dimensional model (assuming a constant length of 35.36 mm) are equal to those of the realistic three-dimensional actuator. This is done because the volume of the actuator strongly affects the resonance characteristics of the device, as discussed in the preceding section. The flow inside the cavity is modeled using the quasi-one-dimensional Euler equations. Both the centerline cut of the three-dimensional actuator and the quasi-one-dimensional geometry are shown in Fig. 1. The region where the quasi-one-dimensional model is used is bounded by the dashed line, whereas in the rest of the domain, the two-dimensional Navier–Stokes equations are solved.

The boundary conditions have been implemented as follows. At the box walls except for the bottom, the Euler wall boundary condition for the normal component of the velocity vector is imposed in the weak sense. The no-slip boundary condition for the velocity vector and a constant wall temperature are imposed on the bottom of the box and on the wall surfaces of the actuator neck. The

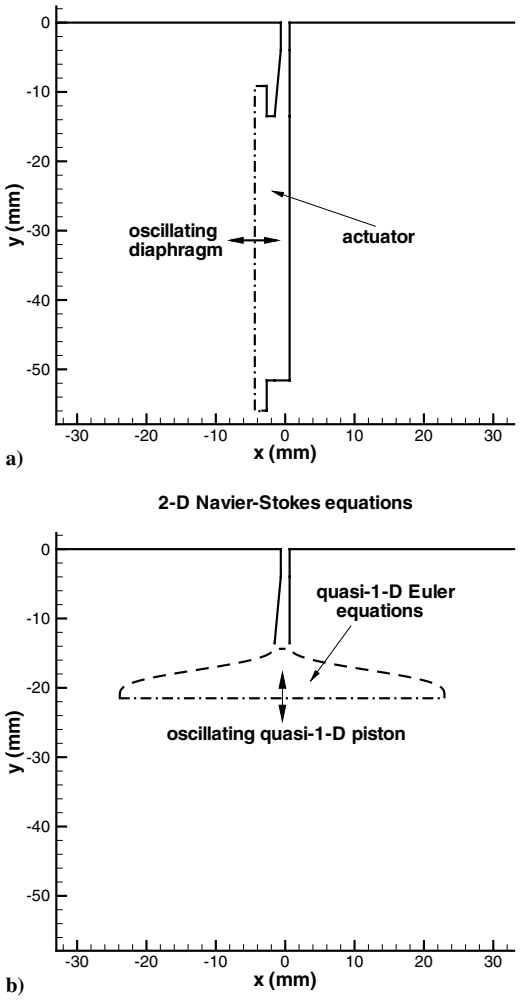

Fig. 1 Actuator geometries: a) centerline cut of the realistic three-dimensional actuator and b) the quasi-one-dimensional geometry used in the numerical simulations.

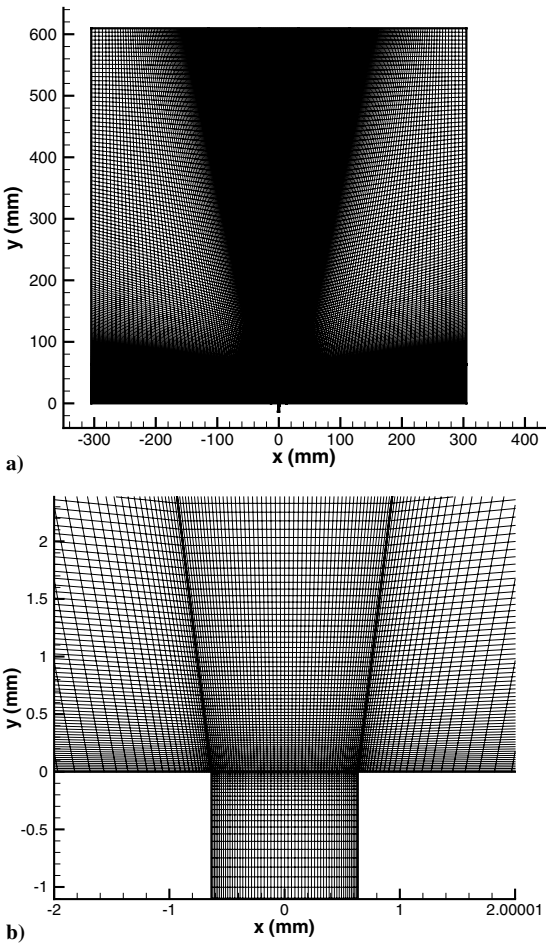

Fig. 2 Computational grid: a) two-dimensional structured grid and b) zoom-in view of the grid near the slot exit.

unsteady flow inside the actuator cavity, generated by the oscillating diaphragm, is modeled by using the reduced-order model briefly described in Sec. III. Note that oscillation of the experimentally determined displacement history at the center of diaphragm is not precisely harmonic. The Fourier transform of the displacement history has shown that there are nonzero high-frequency harmonics in this signal. Because the contribution of the higher harmonics into the overall signal is less than 5%, the diaphragm displacement is assumed to be sinusoidal in time, whereas the higher harmonics have been neglected. To evaluate the diaphragm amplitude used in the moving boundary condition of the quasi-one-dimensional actuator, the shape of the oscillating diaphragm was assumed to be the first mode of the Bessel function eigensolution of the cylindrical symmetric vibration. A scaling factor of 1.35 was later added to obtain the peak exit velocity that was in the Mach = 0.1 range, to replicate the experimental conditions.

The grid is adjusted within the actuator and in the near field of the exterior to achieve three significant digits in the metric coefficients. Figure 2 shows a global view of the two-dimensional structured 12-block grid used in the simulation (Fig. 2a) and a zoom-in view of the grid near the slot exit (Fig. 2b). The exterior grid is sufficient in resolution to accurately resolve the vortices near the slot and up to 20 diameters away from the slot. Beyond that point, the mesh is expanded, and the vortices are allowed to diffuse. To evaluate the accuracy of the numerical solution, three simulations on coarse, medium, and fine grids have been performed. Each finer grid has been obtained from the coarser one by doubling the number of grid points in each spatial direction. Vorticity contours calculated on the coarse, medium, and fine grids after one cycle of diaphragm oscillation are shown in Figs. 3 and 4. As seen in the figures, the coarse-grid solution is very inaccurate and nonsymmetric, whereas the medium-grid solution is in very good agreement with that obtained on the fine mesh. Therefore, all of the simulations presented here were performed on the medium grid containing 98,379 grid points.

A very important question that needs to be addressed is how many periods of diaphragm oscillation should be simulated to replicate this experiment. It is impractical to simulate several thousand diaphragm cycles to generate phase-locked ensemble average data equivalent to that obtained experimentally.[14] To determine the minimum simulation interval necessary to replicate the experiment, the decay rate of the vortices in the exterior chamber should be estimated. A balance exists on average, between the production (device scale) and dissipation (Kolmogorov scale) of vortices in the chamber. The modest Reynolds number of the flow at the slot exit, which is of the order of 2.8×10^3, makes it unlikely that a fully developed turbulent state exists in the chamber. Therefore, the main mechanism for dissipation of vortices generated by the actuator is laminar viscous dissipation. The timescale of the viscous dissipation is of the order of

$$t_{\text{dis}} = l^2/\nu \tag{6}$$

where l is the characteristic length scale of a vortex and ν is the kinematic viscosity. Taking into account that the characteristic length scale is proportional to the orifice width $d = 1.27 \times 10^{-3}$ m and the kinematic viscosity of air at 300 K is 1.55×10^{-5} m^2/s, the characteristic timescale of the vortex kinetic energy decay Eq. (6) is of the order of 0.1 s. Because the viscous dissipation timescale is two orders of magnitude larger than the period of diaphragm vibration and the exterior flow is quiescent, vortices generated during previous cycles remain in the domain and interact with each other for

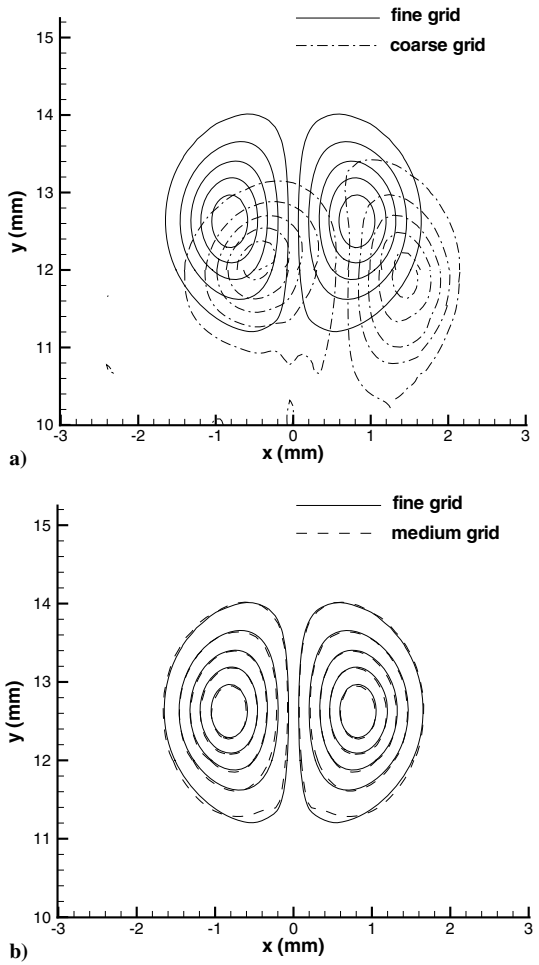

Fig. 3 Vorticity contours 12 mm away from the orifice, calculated on a) the coarse and fine grids and b) the medium and fine grids after one period of diaphragm oscillation.

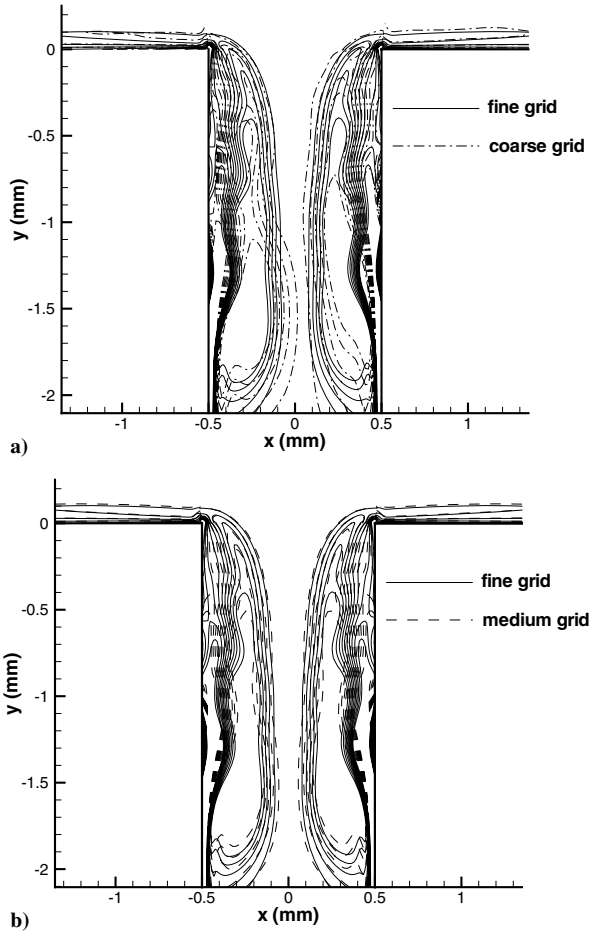

Fig. 4 Vorticity contours inside the neck, calculated on a) the coarse and fine grids and b) the medium and fine grids after one period of diaphragm oscillation.

a long period of time. This vortex–vortex interaction has a strong effect on the synthetic jet properties and should be accurately simulated. The numerical solution is periodic in time only during the first two periods of diaphragm vibration. After two cycles, the vortex-vortex interaction destroys the periodic behavior, and the solution becomes essentially nonperiodic. To obtain statistically significant results, the governing equations should be integrated over at least $\mathcal{O}(10^{-1})$ s that corresponds to $\mathcal{O}(10^2)$ cycles of diaphragm oscillation. Furthermore, the presence of $\mathcal{O}(10^2)$ vortices in the computational domain imposes very severe restriction on the grid resolution. Because of the very large computational cost involved and the limited computer resources available, only 18 cycles of diaphragm oscillation have been simulated.

To evaluate the statistical error obtained after 18 periods of diaphragm oscillations, the v-velocity component averaged over 6, 12, and 18 cycles is shown in Fig. 5. As follows from this comparison, in close proximity to the jet exit the statistically meaningful solution can be obtained after about 10 cycles of diaphragm oscillations. The main reason for such a behavior is that only a few vortices that are near the slot exit have strong effect on the flow characteristics at the orifice. However, this behavior drastically changes in regions away from the slot exit. Figure 5 shows that even after 18 cycles of diaphragm oscillations, the long time-averaged velocity distribution measured at $y = 6$ mm is far from being statistically converged. This result is not surprising because to collect enough statistics in regions located far away from the jet exit the vortex-vortex interaction that occurs in the entire region from the slot exit to the location where the measurement is made should be accurately simulated over several hundred periods of diaphragm oscillations, as discussed in the foregoing paragraph. Therefore, only the comparisons performed in the vicinity of the jet exit are presented here.

To demonstrate the ability of the reduced-order model to predict the three-dimensional actuator dynamics, the phase-averaged time history of the vertical velocity near the center of the slot exit ($x = 0$ mm, $y = 0.1$ mm), obtained with the quasi-one-dimensional model and the HW, PIV, and LDV measurement techniques, is shown in Fig. 6. As one can see in Fig. 6, the numerical results show a good quantitative agreement with the PIV data and a qualitative agreement with the LDV and HW measurements. There is a noticeable discrepancy between the PIV, LDV, and HW data. The numerically predicted phase-averaged v-velocity component at $x = 0$ mm, $y = 2$ mm is compared with the PIV data in Fig. 7. As in the preceding case, the agreement between the numerical and experimental data is good. Note that the HW and LDV data are not available at $y = 2$ mm.

In Fig. 8, the comparison of the long time-averaged v- and u-velocity components across the slot region at $y = 1$ mm, obtained numerically and experimentally, is presented. The numerical solution is not completely symmetric and underpredicts the v-velocity component and overpredicts the u-velocity component as compared with the PIV data. The nonsymmetry of the numerical results indicates that the solution is still in the transition mode, and more periods of diaphragm vibration should be simulated to replicate the experiment.

Figure 9 shows the long time-averaged v-velocity component distribution along the slot centerline, calculated using the quasi-one-dimensional model, which is compared with the PIV and HW data. As already mentioned, the statistically meaningful numerical solution has been obtained only in the vicinity of the jet exit, whereas away from the orifice the solution is far from being statistically

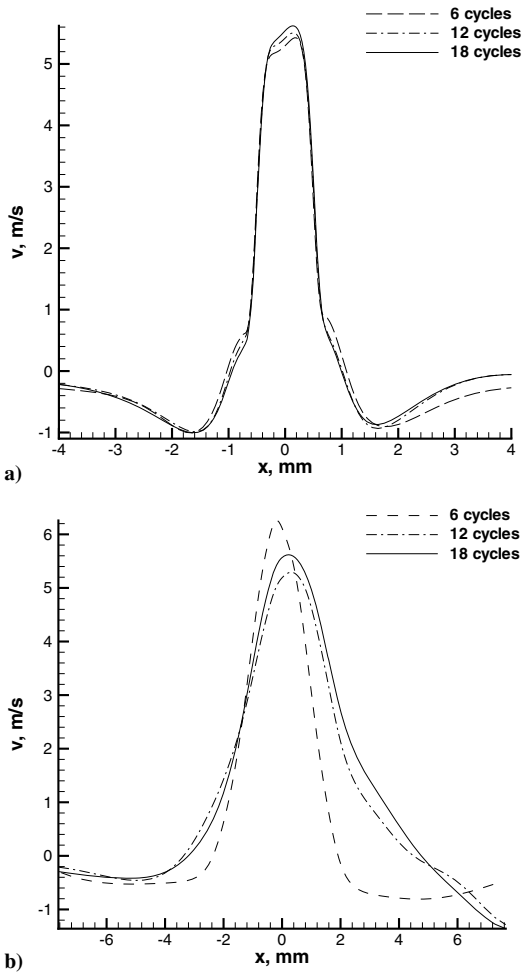

Fig. 5 Long time-averaged v-velocity distributions across the slot at a) $y = 1$ mm and b) $y = 6$ mm, obtained after 6, 12, and 18 cycles of diaphragm oscillations.

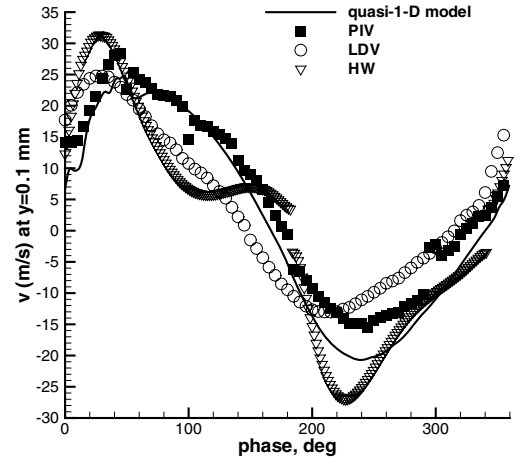

Fig. 6 Time history of the vertical velocity at $x = 0$ mm, $y = 0.1$ mm, obtained with the quasi-one-dimensional model and using the PIV, HW, and LDV measurement techniques.[14]

converged. This behavior can clearly be seen in Fig. 9. For $y < 2$ mm, the numerical results predicted by the quasi-one-dimensional model agree reasonably well with the PIV and HW data. However, farther away from the slot, the numerical solution shows perceptible deviation from both the PIV and HW experimental results. This discrepancy between the numerical and experimental data occurs because the number of cycles simulated is not enough to obtain statistically converged results away from the slot exit.

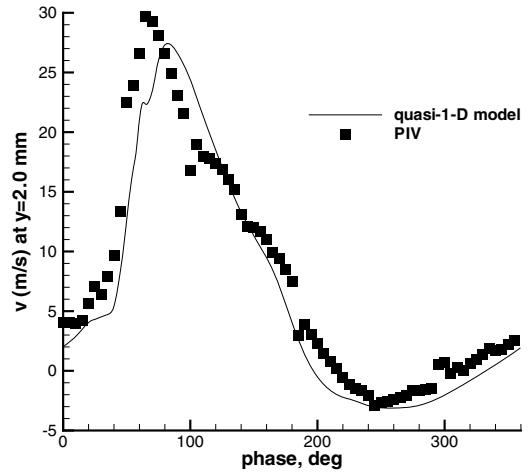

Fig. 7 Time history of the vertical velocity at $x = 0$ mm and $y = 2$ mm, obtained with the quasi-one-dimensional model and the PIV measurement technique.[14]

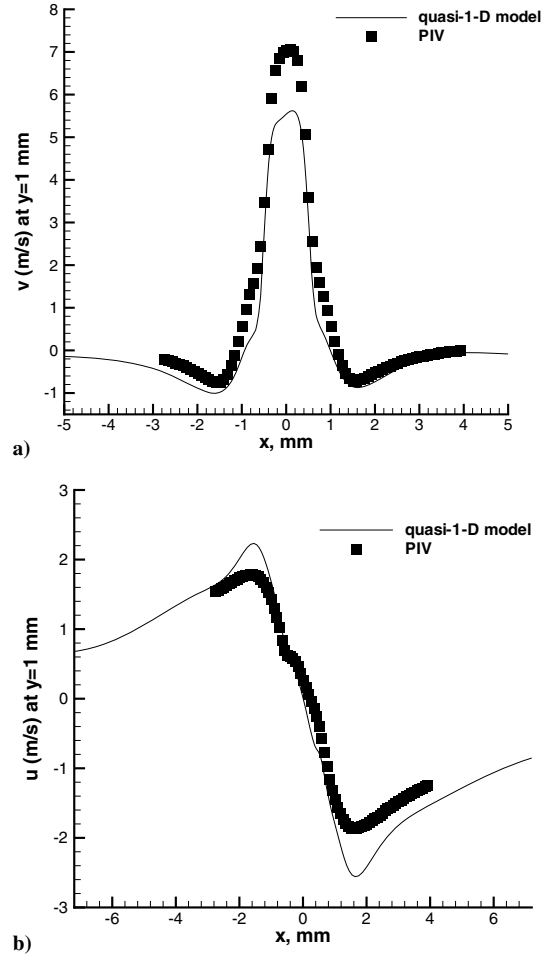

Fig. 8 Long time-averaged a) v-velocity and b) u-velocity distributions across the slot at $y = 1$ mm, obtained with the quasi-one-dimensional model and the PIV measurement technique.[14]

B. Synthetic Jet in Crossflow

The second problem considered is the interaction of the same synthetic jet actuator with a crossflow near a flat plate. The freestream Mach number is chosen to be 0.5, which corresponds to a subsonic regime in the entire flowfield. The actuator geometry as well as its main characteristics, such as the diaphragm amplitude and frequency, remain unchanged and equal to those considered in the preceding problem. For the second test problem, all numerical

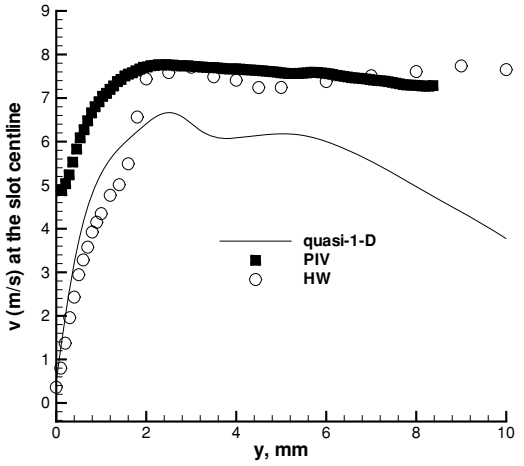

Fig. 9 Long time-averaged v-velocity distribution along the slot centerline, obtained with the quasi-one-dimensional model and the PIV and HW measurement techniques.[14]

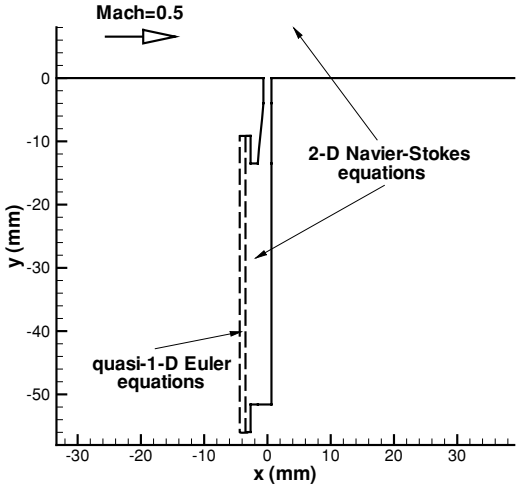

Fig. 10 Full two-dimensional Navier–Stokes model of the realistic actuator.

simulations have been performed on a grid that has practically the same spatial resolution as the mesh used in the quiescent case. In contrast to the synthetic jet in quiescent air, the presence of the crossflow in the problem does not allow vortices expelled from the orifice to accumulate near the jet exit and to have a strong effect on the synthetic jet characteristics. Therefore, only 10 cycles of diaphragm oscillation were calculated to eliminate initial transients and to accumulate meaningful statistics.

For this problem, the governing equations are closed with the following boundary conditions. The velocity vector is set equal to zero, and the temperature is assumed to be constant on the walls. At the subsonic outflow boundary, a boundary condition for the pressure is imposed weakly. Characteristic conditions are applied at the freestream boundary so that the vortex structures can leave the computational domain without producing perceptible spurious reflections. At the inflow boundary, the Blasius profile is used to calculate the conservative variables.

Because there are no experimental data available for this problem, a preliminary assessment of the accuracy of the reduced-order model is made by comparing the numerical solutions obtained with the quasi-one-dimensional model and the full two-dimensional Navier–Stokes simulation of the same actuator. This comparison is less than desirable given the inevitable turbulence of the external flow at the assumed Mach and Reynolds numbers. As discussed earlier, however, for a Reynolds number based on the slot width and the peak jet velocity of about 2.8×10^3, it is unlikely that the flow inside the cavity is turbulent, regardless of whether the flow outside the cavity is essentially turbulent. Furthermore, any turbulent eddies that are ingested during the suction cycle are attenuated inside the cavity and do not dramatically influence the expulsion cycle. Quantification of these assumptions is the topic of ongoing work. Nevertheless, the present study is an important first step.

To avoid the integration of the two-dimensional Navier–Stokes equations on a moving grid, the diaphragm dynamics is simulated by solving the quasi-one-dimensional Euler equations. In other words, the two-dimensional Navier–Stokes equations are employed in the entire actuator cavity, except for a small region near the moving diaphragm that is modeled in a quasi-one-dimensional sense, as shown in Fig. 10. Note that the actual region where the quasi-one-dimensional model is used is smaller than that shown with the dashed line in Fig. 10. This treatment of the moving diaphragm allows us to perform full two-dimensional numerical simulations without using a time-dependent coordinate transformation. Because the region where the quasi-one-dimensional Euler equations are used is much less than that described by the two-dimensional Navier–Stokes equations, this combined approach accounts for the multidimensional and viscous effects inside the actuator cavity and provides high accuracy of the numerical solution. It should be noted that for the quiescent flow problem, this full two-dimensional Navier–Stokes approach is practically inapplicable for measuring the accuracy of the quasi-one-dimensional model because the statistical error component in the first test case is much larger than the error introduced by the reduced-order model itself.

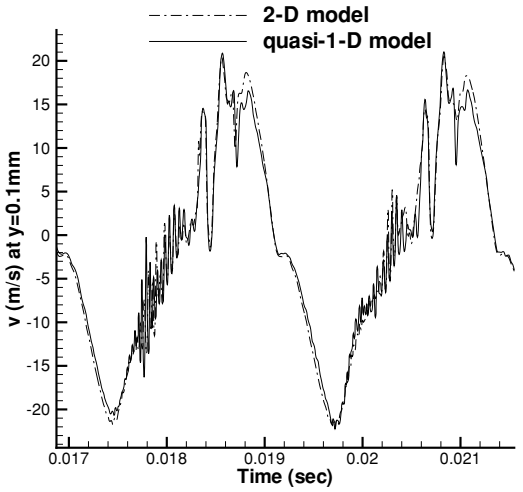

Fig. 11 Time history of the vertical velocity at the slot exit, obtained with the quasi-one-dimensional model and full two-dimensional Navier–Stokes simulation.

The phase-averaged time history of vertical velocity at a location just above the slot exit ($x = 0$ mm, $y = 0.1$ mm), calculated using the reduced-order model and the full two-dimensional Navier–Stokes equations, is shown in Fig. 11. As seen in the figure, the reduced-order model and full two-dimensional Navier–Stokes solutions agree very well. Both numerical solutions are practically periodic except for a quarter of period corresponding to the transition from ingestion to expulsion. The nature of this essentially oscillatory behavior is not well understood and requires additional investigation.

Figure 12 presents phase-locked v-velocity contours calculated using both the full two-dimensional Navier–Stokes equations and the quasi-one-dimensional model at three phase angles of diaphragm oscillation ($\omega t = \pi/4, 3\pi/4, 5\pi/4$). The $\pi/4$ and $3\pi/4$ phase angles correspond to the expulsion stroke, whereas the $5\pi/4$ corresponds to the ingestion stroke. Although the quasi-one-dimensional Euler equations do not take into account the viscous losses and flow separation inside the actuator cavity, the conservation properties of the reduced-order model and the detailed simulation of the

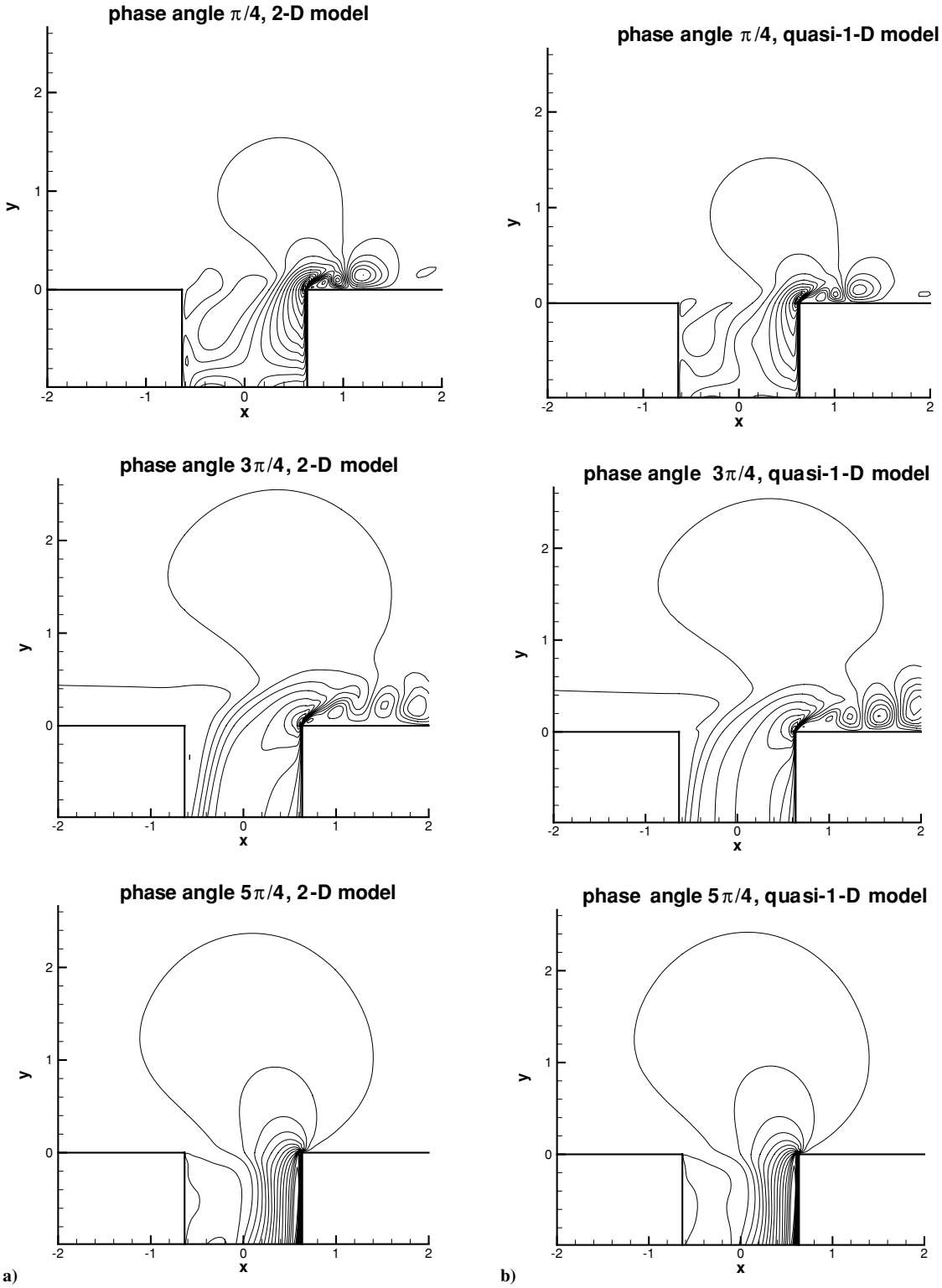

Fig. 12 Phase-locked v-velocity contours obtained with the a) two-dimensional and b) quasi-one-dimensional models at phase angles $\pi/4$, $3\pi/4$, and $5\pi/4$.

multidimensional nonlinear and viscous effects near the slot exit provide good accuracy in the exterior flowfield.

To quantify the magnitude of the error committed by the quasi-one-dimensional model, the comparison of the long time-averaged v- and u-velocity distributions at $y = 0.1$ mm is shown in Fig. 13. Although the quasi-one-dimensional Euler equations do not describe the complex behavior of vortex structures inside the actuator cavity, the velocity profiles obtained with the reduced-order model and the full two-dimensional Navier–Stokes simulation agree to within 3–5%.

Figure 14 presents the long time-averaged normal velocity component distribution along the slot centerline, predicted by both the quasi-one-dimensional and full two-dimensional models. As seen in Fig. 14, the solution obtained with the reduced-order model is almost indistinguishable from the corresponding full two-dimensional Navier–Stokes simulation of the same actuator.

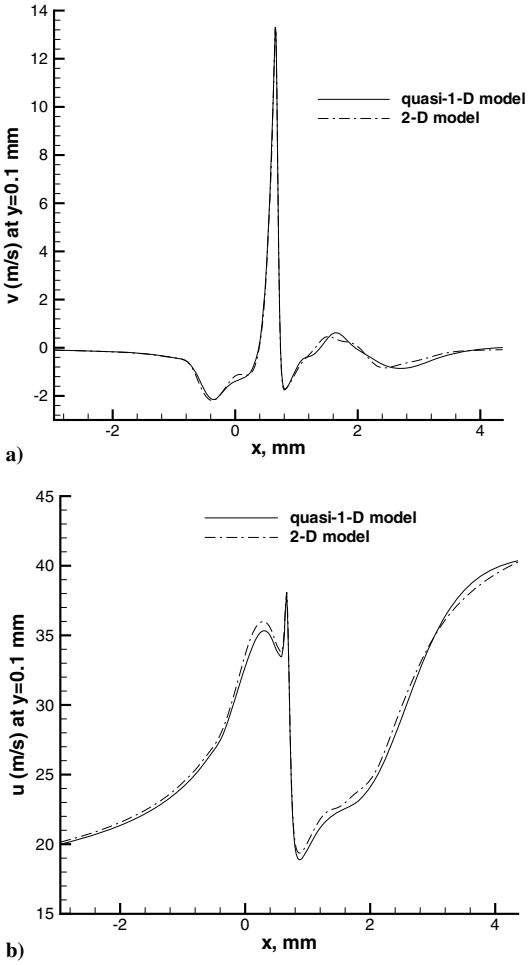

Fig. 13 Long time-averaged a) v-velocity and b) u-velocity distributions across the slot at $y = 0.1$ mm, obtained with the quasi-one-dimensional model and full two-dimensional Navier–Stokes simulation.

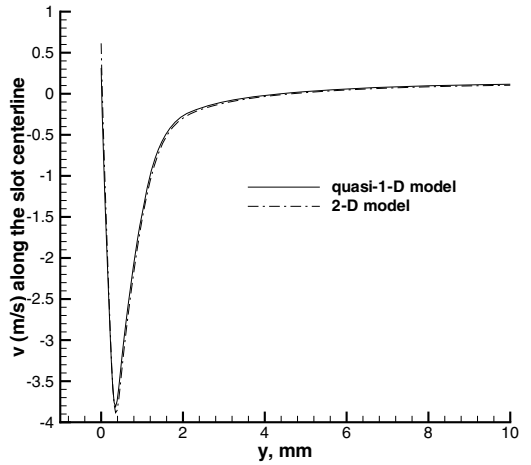

Fig. 14 Long time-averaged of the v-velocity component along the slot centerline, obtained with the quasi-one-dimensional model and full two-dimensional Navier–Stokes simulation.

VI. Conclusions

The systematic methodology for approximating realistic three-dimensional synthetic jet actuators using the quasi-one-dimensional model has been developed. Two test problems, the synthetic jet in quiescent air and the interaction of the same actuator and the subsonic crossflow, have been considered to evaluate the accuracy of the quasi-one-dimensional model for simulating realistic synthetic jet actuators. For the first test problem, the comparison of the numerical results with the experimental data[14] has shown that the reduced-order model provides good accuracy in the vicinity of the jet exit, whereas the discrepancy becomes larger in regions away from the orifice. The main reason for such a behavior is that even after 18 cycles of diaphragm vibrations the numerical solution away from the actuator is not fully statistically converged. For the second test problem, the statistically meaningful solution has been obtained after 10 cycles of diaphragm oscillations. As a result, the numerical solutions obtained with the quasi-one-dimensional model and the full two-dimensional Navier–Stokes simulation of both the interior and exterior flowfields are in a good quantitative agreement not only in the vicinity of the orifice, but also in regions located far away from the jet exit. Summarizing the results presented in this paper and obtained in Ref. 9, the following conclusion can be drawn. The reduced-order model can quantitatively describe the realistic actuator dynamics, if the following criteria are satisfied:

1) The actuator size should be much smaller than the wavelength of diaphragm oscillations.

2) The cavity volume, neck length, slot size, diaphragm area, frequency, and amplitude of the quasi-one-dimensional model should be equal to those of the three-dimensional actuator, whereas the quasi-one-dimensional cavity profile should not exactly coincide with that of the realistic actuator.

3) As has been shown in Ref. 9, the Reynolds number based on the slot size should not be less than 500, and the quasi-one-/two-dimensional interface should be located more than $2d$ away from the orifice exit.

If the preceding constraints are met, then the new quasi-one-dimensional actuator model provides near full fidelity in the exterior flowfield and can be efficiently used for the detailed study of the characteristics of realistic three-dimensional synthetic jet actuators and their application to active flow control.

Acknowledgments

The work of the first author is funded by NASA Langley Research Center and National Institute of Aerospace.

References

[1]Crook, A., Sadri, A. M., and Wood, N. J., "The Development and Implementation of Synthetic Jets for the Control of Separated Flow," AIAA Paper 99-3173, June–July 1999.

[2]Smith, B. L., and Glezer, A., "The Formation and Evolution of Synthetic Jets," *Physics of Fluids*, Vol. 10, No. 9, 1998, p. 2281.

[3]Chen, Y., Liang, S., Aung, K., Glezer, A., and Jagoda, J., "Enhanced Mixing in a Simulated Combustor Using Synthetic Jet Actuators," AIAA Paper 99-0449, Jan. 1999.

[4]Kral, L. D., Donovan, J. F., Cain, A. B., and Cary, A. W., "Numerical Simulation of Synthetic Jet Actuators," AIAA Paper 97-1824, June–July 1997.

[5]Gallas, Q., Mathew, J., Kaysap, A., Holman, R., Nishida, T., Carrol, B., Sheplak, M., and Cattafesta, L., "Lumped Element Modeling of Piezoelectric-Driven Synthetic Jet Actuators," *AIAA Journal*, Vol. 41, No. 2, 2003, pp. 240–247.

[6]Rizzetta, D. P., Visbal, M. P., and Stanek, M. J., "Numerical Investigation of Synthetic Jet Flowfields," *AIAA Journal*, Vol. 37, No. 8, 1999, pp. 919–927.

[7]Mittal, R., and Ramunggoon, P., "On the Virtual Aeroshaping Effect of Synthetic Jets," *Physics of Fluids*, Vol. 14, No. 4, 2002, pp. 1533–1536.

[8]Lee, C. Y., and Goldstein, D. B., "Two-Dimensional Synthetic Jet Simulation," *AIAA Journal*, Vol. 40, No. 3, 2002, pp. 510–516.

[9]Yamaleev, N. K., Carpenter, M. H., and Ferguson, F., "Reduced-Order Model for Efficient Simulation of Synthetic Jet Actuators," *AIAA Journal*, Vol. 43, No. 2, 2005, pp. 357–370.

[10]Carpenter, M. H., Gottlieb, D., and Abarbanel, S., "Time-Stable Boundary Conditions for Finite Difference Schemes Solving Hyperbolic Systems: Methodology and Application to High Order Compact Schemes," *Journal of Computational Physics*, Vol. 111, No. 2, 1994, pp. 220–236.

[11]Carpenter, M. H., Nordström, J., and Gottlieb, D., "A Stable and Conservative Interface Treatment of Arbitrary Spatial Accuracy," *Journal of Computational Physics*, Vol. 148, No. 2, 1999, pp. 341–365.

[12]Nordström, J., and Carpenter, M. H., "Boundary and Interface Conditions for High-Order Finite-Difference Methods Applied to the Euler and Navier–Stokes Equations," *Journal of Computational Physics*, Vol. 148, No. 2, 1999, pp. 621–645.

[13]Carpenter, M. H., and Kennedy, C. A., "Fourth-Order 2N-Storage Runge–Kutta Schemes," NASA TM-109112, April 1994.

[14]Yao, C. S., Chen, F. J., Neuhart, D., and Harris, J., "Synthetic Jet Flow Field Database for CFD Validation," AIAA Paper 2004-2218, June 2004.

C. Rumsey
Guest Editor